Available online at www.sciencedirect.com

SciVerse ScienceDirect

Scripta Materialia 67 (2012) 384–387

Scripta MATERIALIA

www.elsevier.com/locate/scriptamat

# The dead metal zone in high-pressure torsion

Dong Jun Lee,[a] Eun Yoo Yoon,[a] Lee Ju Park[b] and Hyoung Seop Kim[a,*]

[a] *Department of Materials Science and Engineering, Pohang University of Science and Technology (POSTECH), Pohang 790-784, South Korea*

[b] *Agency for Defense Development (ADD), Daejeon 305-152, South Korea*

Received 15 May 2012; revised 19 May 2012; accepted 22 May 2012
Available online 30 May 2012

Plastic deformation behavior during high-pressure torsion (HPT) was analyzed by the finite element method in order to investigate heterogeneous deformation in HPT-processed disks. The effective strain and strain rate developed increase from the center to the edge of the HPT-processed disk; however, they decrease to zero at the surface corner of the disk due to the vertical wall constraint under high pressure, resulting in a stagnant region termed the "dead metal zone".


*Keywords:* High-pressure torsion; Severe plastic deformation; Finite element analysis; Dead metal zone

Severe plastic deformation (SPD) has recently been developed as a "top-down" approach to manufacture bulk ultrafine-grained and nanostructured metallic materials with improved mechanical, physical and multi-functional properties [1–3]. Among various SPD processes, high-pressure torsion (HPT) is perhaps the most effective for grain refinement, since extraordinarily large strain and high pressure can be imparted to workpieces more easily compared to other SPD processes [4], such as the well-known equal channel angular pressing and accumulative roll-bonding processes.

The concept of HPT was first proposed more than 70 years ago [5], and has been investigated with respect to grain refinement in the past decade. The HPT process consists of two stages [6]: an initial compression stage using the high pressure imposed by the die and a subsequent torsion stage, during which the high pressure is maintained. A large amount of shear deformation is imposed on a disk-shaped workpiece by multiple rotations of the die during the torsion stage. The equivalent (effective) strain, $\epsilon$, generated in the workpiece by simple torsion is given by

$$\epsilon = \frac{\gamma}{\sqrt{3}} = \frac{r\theta}{\sqrt{3}h} \tag{1}$$

Where $\gamma$ is the shear strain, $r$ is the radial distance from the center of the disk-shaped workpiece, θ is the rotation angle and $h$ is the thickness of the workpiece. It should be noted that plastic deformation in the workpiece is independent of the vertical position under simple torsion. However, the real strain generated in the workpiece during HPT should be different from the torsion strain due to compression by high pressure and to non uniform strain by the special geometry of HPT dies. Therefore, a local deformation analysis using the finite element method (FEM) should be carried out to investigate plastic deformation during HPT. Several papers [7–10] have analyzed the plastic deformation during HPT using the FEM and reported a change in thickness of the specimen, elastic recovery, the effect of the friction coefficient, mean stress, torque etc. It is now necessary to focus on strain distribution inside the workpiece in order to better understand HPT processing and the material's response to the dies in HPT.

In this paper, FEM analysis coupled with a constitutive model based on a dislocation cell evolution mechanism of plastic deformation was employed in order to understand local deformation of a workpiece during HPT. In particular, a "dead metal zone" (DMZ) phenomenon at the edge corner of the workpiece during the HPT process was found and discussed in light of experimental evaluations of the deformed geometry and microstructures.

Isothermal FEM simulations of the HPT process were carried out using the commercial rigid–plastic finite element code, DEFORM-3D ver. 6.1 [11]. A user-defined material subroutine for the three-dimensional

* Corresponding author. Tel.: +82 54 279 2150; fax: +82 54 279 3150; e-mail: hskim@postech.ac.kr

1359-6462/$ - see front matter © 2012 Acta Materialia Inc. Published by Elsevier Ltd. All rights reserved.
http://dx.doi.org/10.1016/j.scriptamat.2012.05.024

version of the dislocation density-based constitutive model [12,13] was employed. The parameters of the constitutive model were determined for the best fitted stress–strain curve from the tensile test of copper and selected from Refs. [13,14]. For details of the constitutive model, the reader is referred to Refs. [12–15].

The initial dimensions of the workpiece were 10 mm diameter and 1.5 mm thickness. The number of initial meshes for the workpiece was 150,000, which was sufficient to show the local deformation behavior. The upper and lower anvils of the die had depressions of 10 mm diameter and 0.25 mm thickness. The lateral wall was set at an angle of 5° to the vertical. In the compression stage, the speed of the top anvil was 0.1 mm $s^{-1}$ until a pressure of 6 GPa was developed on the workpiece. In the torsion stage, the lower anvil was rotated at 0.1 rad $s^{-1}$ up to a full turn with a constant pressure of 6 GPa. The friction between the die and the workpiece was set to satisfy the sticking condition, since the roughness of the die surface was high enough to prevent slippage between the workpiece and the die.

Figure 1(a) shows deformed geometries with effective strain distributions for the initial stage, the compression stage, after 1/2 turn and after 1 turn in HPT. The effective strain is seen to increase as the number of turns increases. According to a general theory of torsion deformation, given by Eq. (1), the torsional strain $\gamma$ should be proportional to the radial distance $r$ from the vertical axis and have the same value along the thickness direction, as indicated by the dashed lines in Figure 1(b). Moreover, there should be no strain developed by torsional deformation at the center of the workpiece ($r = 0$). However, compressive strains are developed during the torsion stage as well as the compression stage in HPT. During the compression stage, for the pressure of 6 GPa pressure in the present simulations, the effective strain reached a value of 0.5 at the center and over 1 near the workpiece edge (Fig. 1(b)) due to the flow of the material toward the flash region. A higher strain in the edge region after the compression stage was identified in the analysis by Song et al. [6].

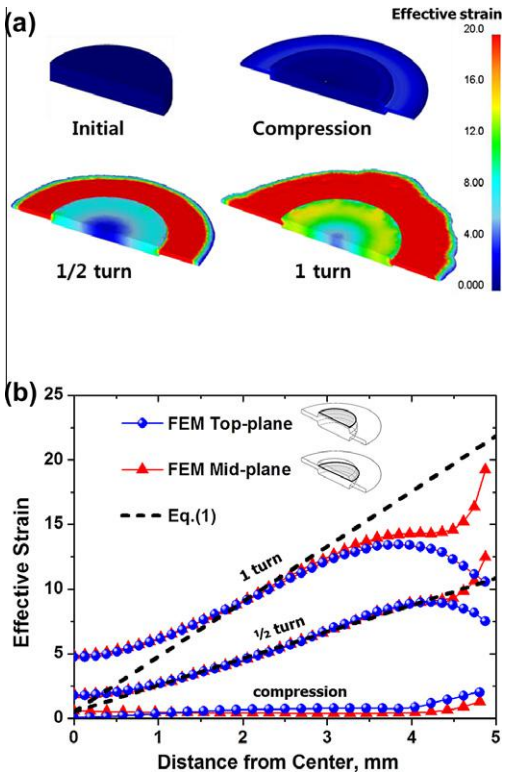


**Figure 1.** (a) Deformed geometries at the initial stage, after compression, after 1/2 turn and after 1 turn with effective strain distributions. (b) Path plots of the effective strain on the top plane and mid-plane after compression, 1/2 turn and 1 turn, comparing the theoretical strain and the results from FEM simulations.

The effective strains from the FEM results at the center increase to 1.8 and 5 after half a turn and a full turn, respectively, while the torsion (shear) strain given by Eq. (1) is zero. The strain obtained by the FEM simulations at the center, which is higher than the theoretical value corresponding to Eq. (1), can be explained by (i) the compression mode in HPT and (ii) the finite mesh size in the FEM. First, during the rotation stage, the thickness of the specimen continues decreasing due to the constant applied pressure of 6 GPa, which results in a continuous evolution of the compressive strain. In the FEM simulation, under 6 GPa, the initial thickness of 1.5 mm decreased to 1.14 mm after compression and 1.02 mm after one turn HPT. Second, according to the torsion theory, the *point* of zero torsional strain is at the axis of rotation. However, a *volumetric* (not a point) element in the center in the FEM includes the center point and neighboring regions. Therefore, the center volumetric element cannot have zero volume and zero deformation.

The FEM simulation and torsion theory results are in a good agreement in the vicinity of middle of the disk ($r = 2$–$3$ mm) after a full turn and in the $r = 0.5$–$4$ mm region after half a turn. However, at the edge region ($r = 4.5$–$5$ mm), the results of the FEM simulations deviate from the theoretical values. The effective strains in both the top and mid-planes increase along the radial direction up to approximately 4 mm radius, and the effective strain in the mid-plane continues increasing; in particular, the strain rapidly increases near the edge region, while it decreases in the top plane (and also in the bottom plane). To explain this strain separation, the effective strain rate from the FEM simulations during the torsional stage was examined, as shown in Figure 2.

The effective strain rate during the torsion stage is also proportional to the distance from the center. However, a low strain rate region can be observed around the edge corner of the workpiece, as indicated by the blue region in Figure 2(a), as well as in the center. The cut plane view of Figure 2(a) clearly shows the low deformation zone in the corner of the top plane. In contrast, there is a high strain rate region near the edge in the mid-plane. Figure 2(b) shows path plots of the effective strain rate from the center to the edge for the top plane (triangular symbol) and the mid-plane (circular symbol), together with the theoretical effective strain rate (dashed line). The theoretical effective strain rate, $\dot{\epsilon}$, is given by,

$$\dot{\epsilon} = \frac{\dot{\gamma}}{\sqrt{3}} = \frac{r}{\sqrt{3}h} \cdot \frac{d\theta}{dt} \tag{2}$$

Where $\dot{\gamma}$ is the shear strain rate and $t$ is time. In the present FEM simulations, the rotational speed of the lower

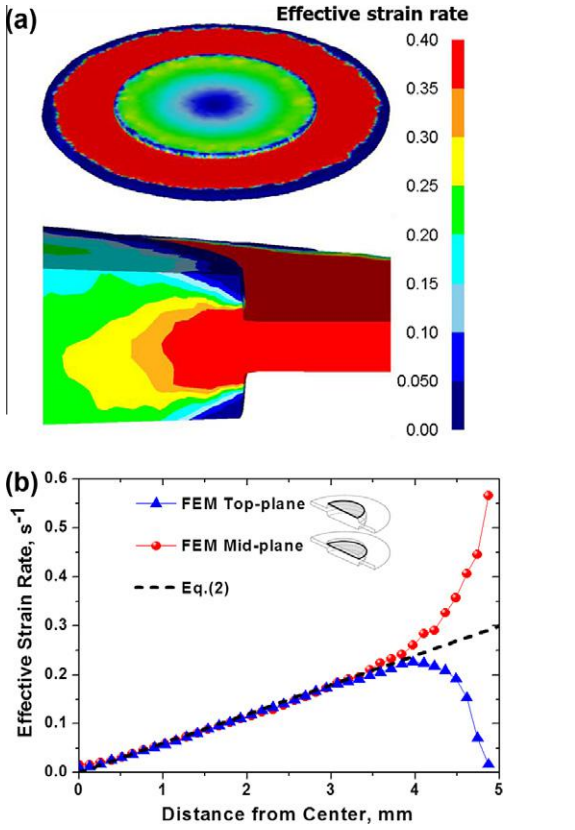


**Figure 2.** (a) Distribution of effective strain rate during torsion; (b) path plots of the effective strain rate from the center to the edge on the top plane and the mid-plane.

die was set to be 0.1 rad $s^{-1}$. The theoretical value and the results from the FEM analyses are in good agreement in the $r = 0$–4 mm inner region, while the edge region shows totally different trends and values. That is, the effective strain rate in the mid-plane increases with the radius, whereas the top plane strain rate decreases with the radius from $r = 4$ mm on, as in the effective strain distributions in Figure 1. This strain rate separation phenomenon, where the strain rate (ultimately the total strain) decreases and increases with the radius in the top and mid-planes around the edge, respectively, can be explained by surface traction in the workpiece.

During HPT, normal traction (defined as the force acting on the surface per unit area of the deformed solid) is imposed on the workpiece along the axial direction. If this normal traction is large enough to induce a high friction force and high shear traction, a sticking condition between the workpiece and the die is fulfilled and there is no slippage during punch rotation. Due to the sticking of the workpiece in the die face, a stagnant zone is generated in the corner region. This stagnant zone, where there is almost negligible strain rate and strain by the sticking interface during HPT, is defined as the DMZ of the workpiece, and is shown in a schematic illustration in Figure 3. The edge region on the mid-plane, in contrast, shows much higher effective strain and strain rate than the inner region, since there is little constraint in the mid-plane of the edge. Therefore, the

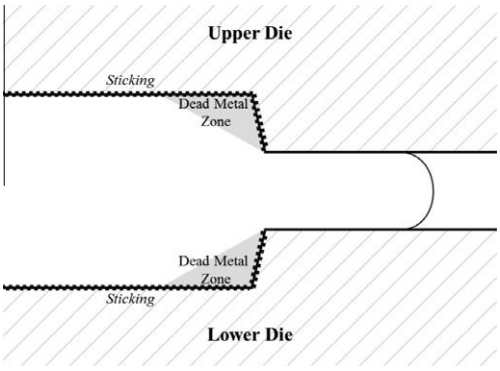


**Figure 3.** A schematic diagram showing the dead metal zone in HPT.

deformation is concentrated on the mid-plane near the edge. The occurrence of a DMZ was also found in hot extrusion under high friction [16].

The DMZ phenomenon can be verified via fracture occurring in the case of magnesium alloy AZ31. Magnesium alloys mostly exhibit poor formability due to a hexagonal close-packed crystal structure that has insufficient slip systems, and are prone to fracture during SPD at room temperature [17–19]. Interestingly, ring-shaped fragmentation occurred during HPT for one turn under 6 GPa, as shown in Figure 4(a). The separated ring piece corresponds to the stagnant region (DMZ), as shown in Figure 2. In order to examine the microstructural differences between the internal disk piece and the ring-shaped

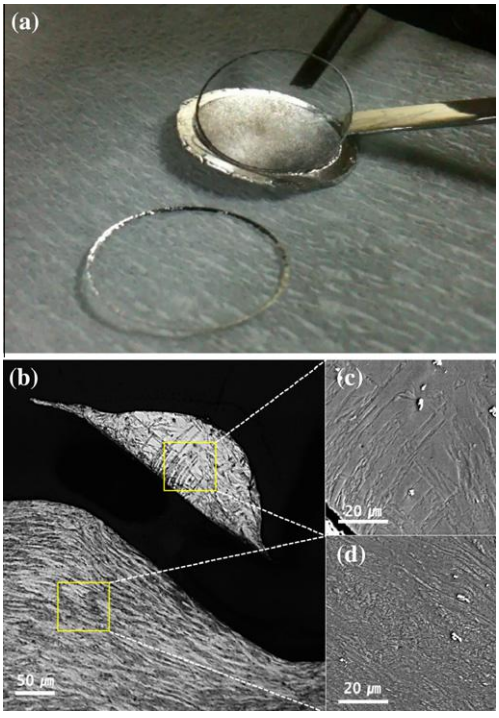


**Figure 4.** Experimental evidence of a dead metal zone in magnesium alloy (AZ31). (a) Photograph of a ring-shaped fragmented part during the torsion stage at the edge of the specimen. (b) The difference in microstructures between the inner part and the broken DMZ piece. Scanning electron microscopy images showing (c) the partly deformed DMZ piece and (d) the heavily deformed inner part.

fragmented piece, the cross-sectional area of the disk was polished and examined. The fine polished pieces were etched to reveal the grain boundaries and observed for microstructural features using an optical microscope (Olympus BX51 M), as presented in Figure 4(b), and a scanning electron microscope (Hitachi SU 6600), as shown in Figure 4(c) and (d). Figure 4(b)–(d) clearly presents differences in microstructures: the inner piece shows heavily deformed flow lines and a microstructure refined by SPD, while the separated ring piece shows a less deformed microstructure, with coarse grains remaining. The coarse-grained microstructure in the separated ring indicates that the separation occurred at a nearly stage of the deformation processing and was hardly influenced by torsional deformation.

Furthermore, the results of the bulk HPT sample [20,21] indicate that the deformation in HPT was concentrated on the mid-plane. The top and bottom surface regions, in contrast, experienced less deformation and had a large grain size. This strain inhomogeneity in the bulk sample having a less deformed region of 8 mm thickness is another extreme case of the DMZ phenomenon, i.e. a large area of DMZ due to deep depression of the die. Thus, it can be concluded that the wall geometry of the HPT die has a critical effect on the DMZ phenomenon and plays a significant role in the strain homogeneity of HPT.

In summary, in order to understand the heterogeneous plastic deformation in an HPT-processed disk, a finite element analysis was employed. The plastic deformation was highly non uniform along the thickness direction due to the die geometry and high friction, as well as along the radial direction due to the characteristics of torsion. Plastic deformation increased from the center to the edge in the middle region in the thickness direction of the HPT-processed disk, while it dropped to zero in the stagnant region or "dead metal zone" at the surface corner of the disk due to the vertical wall constraint under high pressure.

This study was supported by A.D.D. through basic research Project (11-01-04-08).

[1] R.Z. Valiev, R.K. Islamgaliev, I.V. Alexandrov, Prog. Mater. Sci. 45 (2000) 103.
[2] M.A. Meyers, A. Mishra, D.J. Benson, Prog. Mater. Sci. 51 (2006) 427.
[3] R.Z. Valiev, T.G. Langdon, Prog. Mater. Sci. 51 (2006) 881.
[4] A.P. Zhilyaev, T.G. Langdon, Prog. Mater. Sci. 53 (2008) 893.
[5] P.W. Bridgman, J. Appl. Phys. 14 (1943) 273.
[6] Y. Song, E.Y. Yoon, D.J. Lee, J.H. Lee, H.S. Kim, Mater. Sci. Eng. A 528 (2011) 4840.
[7] H.S. Kim, J. Mater. Process. Technol. 113 (2001) 617.
[8] H.S. Kim, S.I. Hong, Y.S. Lee, A.A. Dubravina, I.V. Alexandrov, J. Mater. Process. Technol. 142 (2003) 334.
[9] S.C. Yoon, Z. Horita, H.S. Kim, J. Mater. Process. Technol. 201 (2008) 32.
[10] R.B. Figueiredo, P.R. Cetlin, T.G. Langdon, Mater. Sci. Eng. A 528 (2011) 8198.
[11] DEFORM software, Scientific Forming Technologies Corp., Columbus, OH, 2007.
[12] L.S. Tóth, A. Molinari, Y. Estrin, J. Eng. Mater. Technol. 124 (2002) 71.
[13] S.C. Baik, Y. Estrin, H.S. Kim, R.J. Hellmig, Mater. Sci. Eng. A 351 (2003) 86.
[14] Y. Estrin, L.S. Tóth, A. Molinari, Y. Bréchet, Acta Mater. 46 (1998) 5509.
[15] Y. Estrin, H. Mecking, Acta Metall. 32 (1984) 57.
[16] K. Laue, H. Stenger, Extrusion: Processes, Machinery, Tooling, ASM International, Metals Park, OH, 1981, p. 8.
[17] M.G. Kang, T.I. So, H.C. Jung, K.S. Shin, Korean J. Met. Mater. 49 (2011) 686.
[18] S.C. Yoon, C.H. Bok, M.H. Seo, T.S. Kim, H.S. Kim, Mater. Trans. 49 (2008) 963.
[19] D.H. Kim, H.K. Lim, Y.K. Kim, J.S. Kyeong, W.T. Kim, D.H. Kim, Metal. Mater. Interact. 17 (2011) 383.
[20] G. Sakai, K. Nakamura, Z. Horita, T.G. Langdon, Mater. Sci. Eng. A 406 (2005) 268.
[21] Z. Horita, T.G. Langdon, Scripta Mater. 58 (2008) 1029.